

Chiral tunneling of topological states: towards the efficient generation of spin current using spin-momentum locking

K. M. Masum Habib,* Redwan N. Sajjad, and Avik W. Ghosh
*Department of Electrical and Computer Engineering
University of Virginia, Charlottesville, VA 22904*

We show that the interplay between chiral tunneling and spin-momentum locking of helical surface states leads to spin amplification and filtering in a 3D Topological Insulator (TI). Chiral tunneling across a TI pn junction allows normally incident electrons to transmit, while the rest are reflected with their spins flipped due to spin-momentum locking. The net result is that the spin current is enhanced while the dissipative charge current is simultaneously suppressed, leading to an extremely large, gate tunable spin to charge current ratio (~ 20) at the reflected end. At the transmitted end, the ratio stays close to one and the electrons are completely spin polarized.

Since their theoretical prediction and experimental verification in quantum wells and bulk crystals, Topological Insulators have been of great interest in condensed matter physics, even prompting their classification as a new state of matter[1]. The large spin orbit coupling in a TI leads to an inverted band separated by a bulk bandgap. Symmetry considerations dictate that setting such a TI against a normal insulator (including vacuum) forces a band crossing at their interface, leading to gapless edge (for 2D) and surface (for 3D) states protected by time reversal symmetry. At low energies, the TI surface Hamiltonian $H = v_F \hat{z} \cdot (\boldsymbol{\sigma} \times \mathbf{p})$ [1] resembles the graphene Hamiltonian $H = v_F \boldsymbol{\sigma} \cdot \mathbf{p}$ except that the Pauli matrices in TI represent *real*-spins instead of *pseudo*-spins in graphene. This suggests that the chiral tunneling (the angle dependent transmission) in a graphene pn junction[2–5] is expected to appear in a TI pn junction (TIPNJ) as well. Although TIPNJs have been studied recently[6–8], the implication of chiral tunneling combined with spin-momentum locking in spintronics has received little attention.

The energy dissipation of a spintronic device strongly depends on the efficiency of spin current generation. The efficiency is measured by the spin-charge current gain $\beta = \frac{2I_s/\hbar}{I_q/q}$, where I_s and I_q are the non-equilibrium spin and charge currents respectively. Increasing β reduces the energy dissipation quadratically. The gain for a regular magnetic tunnel junction is less than 1[9]. The discovery of Giant Spin Hall Effect (GSHE)[10] shows a way to achieve $\beta > 1$ by augmenting the spin Hall angle θ_H with an additional geometrical gain[11]. The intrinsic gain θ_H for various metals and metal alloys has been found to vary between 0.07-0.3[10, 12, 13]. Recently, Bi_2Se_3 based TI has been reported to have ‘spin torque ratio’ (a quantity closely related to θ_H) of 2-3.5[14] and has been shown to switch a soft ferromagnet at low temperature[15]. An oscillatory spin polarization has also been predicted in TI using a step potential[16].

In this letter, we show that the interplay between the chiral tunneling and spin momentum locking in TIPNJ

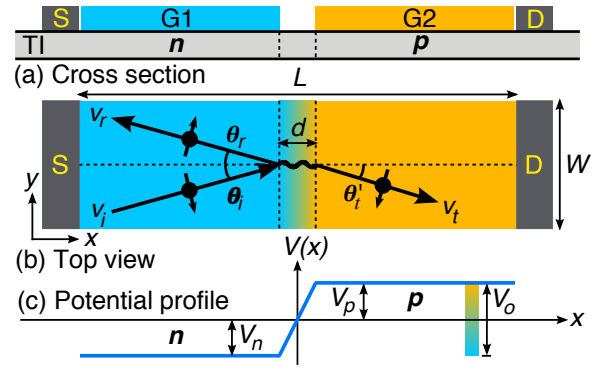


FIG. 1. (Color online) (a) Cross section of the TIPNJ. The source, the drain and the gates are placed on the top surface of the 3D TI. The spatially separated gates create a graded pn junction. (b) Top view of the device showing the directions of incident, reflected and transmitted electrons and their spins. The spin of the reflected wave is flipped due to spin-momentum locking which enhances the spin current at source. (c) Linear approximation of potential energy profile.

shown in Fig. 1 leads to an extremely large, electrically tunable spin-charge current gain β even without utilizing any geometric gain. The chiral tunneling in TIPNJ only allows electrons with very small incident angle to pass through and all other electrons are reflected back to the source in the same way as graphene. As a result, charge current going through the junction decreases. Due to spin-momentum locking, the injected electrons have down spin but the reflected electrons have up spin, which enhances the spin current at the source contact. These result in a gate tunable, extraordinarily large spin-charge current gain. We show below that in a split-gate, symmetrically doped TIPNJ, the spin-charge current gain is,

$$\beta \approx \frac{1 + R_{av}}{1 - R_{av}} \approx \pi \sqrt{\frac{qV_o d}{\hbar v_F}} \quad (1)$$

at the source contact for small drain bias. Here, R_{av} is the reflection probability averaged over all modes, V_o is the built in potential of the TIPNJ and d is the split

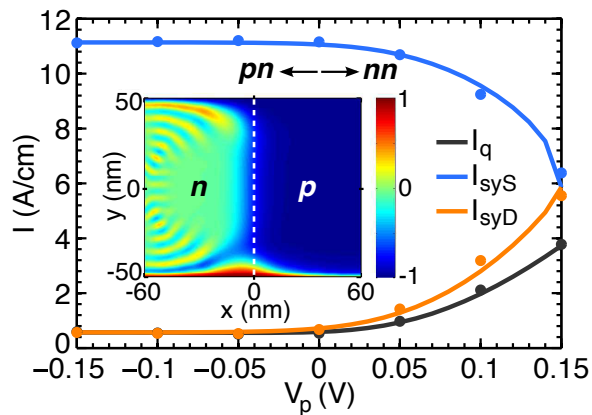


FIG. 2. (Color online) Charge and spin current vs. gate voltage on the p -side (V_p) at $V_n = 0.15$ V. The charge and spin currents at drain are reduced whereas the spin current at source is enhanced as the device is driven from nn ($V_p = 0.15$ V) to pn ($V_p = -0.15$ V) regime. The analytical (solid lines) and the NEGF (circles) results are in good agreement. **Inset:** Spin polarization in symmetric pn regime. In the p region only transmitted modes (spin down) exist resulting in strong polarization (blue). In the n region, both the incident (spin down) and the reflected modes (spin up) exist, hence it is mostly unpolarized (green).

between the gates. For large bias, Eq. 1 can be approximated as $\beta \approx 2\sqrt{qV_o d/\hbar v_F}$. In a typical TIPNJ with $d = 100$ nm, $V_o = 0.3$ V and $v_F = 0.5 \times 10^6$ m/s, β at source is ~ 30 for small bias and ~ 20 for large bias. At drain, β remains close to 1. We also show below that the p region is highly spin polarized since only the small angle modes (with spin- y) exist there. The large β in a TIPNJ does not require any geometrical gain and can potentially be larger than the net gain in GSHE systems like β -Ta and W[17] that rely on the additional geometrical gain. In addition, it is gate tunable, meaning that we can turn its value continuously from 1.5 to 20. The directions of spin and charge are parallel in TIPNJ, as opposed to the transverse flow in GSHE.

The cross section and the top view of the model TIPNJ device are shown in Fig. 1a and 1b respectively. The 3D TI is assumed to be Bi_2Se_3 which has the largest bulk bandgap of 350 meV. The source (S) and the drain (D) contacts are placed on the top surface of the TI slab. We assume that the electron conduction happens only on the top surface. This is a good approximation since the device is operated within the bulk bandgap to minimize the bulk conduction and we numerically verified that only a small part of the total current goes through the side walls which was also seen in experiment[18]. The p and n regions are electrically doped using two external gates G1 and G2 separated by the split distance d . Such gate controlled doping of TI surface states has been demonstrated experimentally for Bi_2Se_3 [19]. The device has a built-in potential $V_o = V_p + V_n$ distributed between the p and n

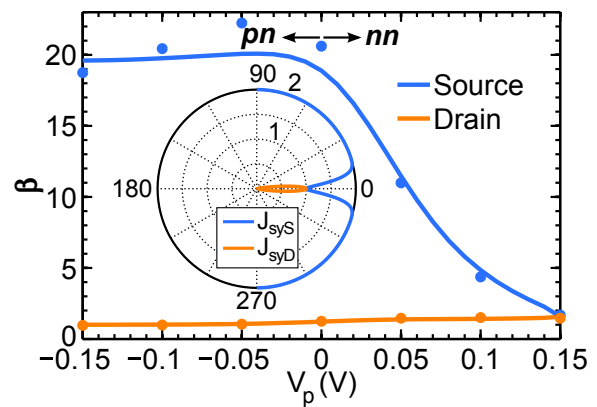


FIG. 3. (Color online) Spin-charge current gain β vs. V_p at $V_n = 0.15$ V. β increases at source as the device is driven from nn to pn regime. The solid lines and the circles represent analytical and NEGF results respectively. **Inset:** Angle dependent normalized spin current densities at source and drain in symmetric pn regime. Spin current at drain (J_{syD}) is carried by small angle modes only. All other modes contribute to source spin current (J_{syS}) twice: (1) when they are injected and (2) when they are reflected since their spins are flipped.

regions as shown in Fig. 1c assuming a linear potential profile inside the split region. Electrons are injected from source and collected at drain by a bias voltage V_{DS} .

Although an equilibrium spin current exists on the TI surface, it has no consequences for the measurable spin current[20, 21]. Therefore, we only considered the non-equilibrium spin current. There has been a lot of discussions on the equilibrium spin current in the literature[22–25]. In this article, we choose a biasing scheme that defines the equilibrium state. We connect the drain contact to the ground and reference the gates with respect to the ground so that $\mu_D = 0$ and $\mu_S = qV_{DS}$ where μ_D and μ_S are the chemical potentials of the drain and the source contacts respectively. The equilibrium current, I_{s_0} is then defined by $V_{DS} = 0$ and $\mu_D = \mu_S = 0$. The non-equilibrium spin current is obtained by subtracting I_{s_0} from the total spin current calculated for nonzero bias ($\mu_D = 0$ and $\mu_S = qV_{DS}$). A detailed description of this method is discussed in the Supplement.

The spin current, the charge current and the spin to charge current ratio are shown in Figs. 2-3 as functions of gate bias of the p region. The solid lines were calculated using Eqs. 2-4 and S3 evaluated at the source and drain contacts. The discrete points were calculated using the non-equilibrium Green's function (NEGF) formalism and the discretized k.p Hamiltonian which captures the effects of edge reflections. Both analytical and numerical simulations were done for a device with length $L = 120$ nm, width $W = 100$ nm, split length $d = 100$ nm, drain bias $V_{DS} = 0.1$ V, gate voltage $V_n = 0.15$ V at room temperature. When the gate voltage of p region $V_p = 0.15$ V, the channel is a perfect nn type with uniform poten-

tial profile. Thus, all the modes are allowed to transmit from the source to the drain and there is no reflection. Hence, the charge current is maximum, spin current at the source and drain are equal and $\beta = \pi/2$ as shown in Fig. 3. When the gate voltage V_p is decreased to -0.15 V, the potential profile is no longer uniform, the channel becomes a pn junction and most of the electrons are reflected back from the junction and therefore, charge current is reduced. Since the incident and reflected waves have opposite spins, the reflected waves enhances the spin current at the source end and β becomes large at the source contact. In the drain contact, however, only the transmitted electrons are collected and β remains close to 1. Thus, β changes from 1.5 to 20 at source contact and remains close to 1 at the drain when the device is driven from the nn to the pn regime. The agreement between the numerical and the analytical results shown in Figs. 2 and 3 indicates that the physics described here is robust against the edge reflection at finite drain bias and room temperature.

Let us now derive Eq. 1 and analyze the underlying physics. We start with the effective Hamiltonian for 3D TI surface states and follow the similar procedure as described in Ref.[26] to obtain the continuity equation for spin, $\frac{\partial \mathbf{s}}{\partial t} = -\nabla \cdot \hat{\mathbf{J}}_{\mathbf{s}} + \hat{\mathbf{J}}_{\omega}$. Here, $\hat{\mathbf{J}}_{\mathbf{s}}$ is a rank 2 tensor describing the translational motion of spin and $\hat{\mathbf{J}}_{\omega}$ is a vector describing the rate of change of spin density due to spin precession at location \mathbf{r} and time t . The quantity $\hat{\mathbf{J}}_{\omega}$ is also referred to as spin torque[26]. Among nine elements of $\hat{\mathbf{J}}_{\mathbf{s}}$, only $\hat{J}_{sy}^x = -\frac{\hbar v_F}{2} \mathbf{I}$ and $\hat{J}_{sx}^y = \frac{\hbar v_F}{2} \mathbf{I}$ are nonzero for TI. The current density operator J_{sy}^x describes spin current carried by spin- y along \hat{x} direction etc. Inside the gate regions where there is no scattering, the angular term \mathbf{J}_{ω} is zero and the spin current is conserved. However, at the pn junction interface, electrons are reflected which is accompanied by a change in the spin angular momentum. As a result, inside the pn junction interface, $\mathbf{J}_{\omega} \neq \mathbf{0}$ and the spin current is not conserved (see the Supplement). At steady state, $\nabla \cdot \hat{\mathbf{J}}_{\mathbf{s}} = \hat{\mathbf{J}}_{\omega}$ and hence, for the two terminal device shown in Fig. 1, the difference between the spin currents at the source and the drain terminal is the spin torque generated by the TIPNJ. Similarly, we obtain the charge current density operators $\hat{J}^x = -qv_F \sigma^y$ and $\hat{J}^y = qv_F \sigma^x$ where \hat{J}^x describes the motion of electrons moving along the \hat{x} direction. For the TIPNJ, since there is no net charge or spin transfer in \hat{y} direction, $J_{sx}^y = 0$ and $J^y = 0$.

The wavefunction of an electron in the n side ($x < -d/2$) of the TIPNJ shown in Fig. 1 can be expressed as $|\psi\rangle = |\psi_i\rangle + r|\psi_r\rangle$ where $|\psi_i\rangle$ is the incident wave, $|\psi_r\rangle$ is the reflected wave and r is the reflection coefficient. The general form of spin-momentum locked incident wave with incident angle θ_i and energy E is $|\psi_i\rangle = 1/\sqrt{2A} (1 - s_i i e^{i\theta_i})^T e^{i\mathbf{k}_i \cdot \mathbf{r}}$ where $A = WL$ is the area of the device, \mathbf{k}_i is the wavevector with mag-

nitude $k_i = \frac{|E+qV_n|}{\hbar v_F}$ and direction θ_i and $s_i = \text{sgn}(E + qV_n)$. Similarly, the reflected wave is given by $|\psi_r\rangle = 1/\sqrt{2A} (1 - s_i i e^{i\theta_r})^T e^{i\mathbf{k}_r \cdot \mathbf{r}}$ where $k_r = k_i$ and $\theta_r = \pi - \theta_i$. In the p side ($x > d/2$), only the transmitted wave exist. Hence, the wave function of electron is expressed as $|\psi\rangle = t|\psi_t\rangle$ with $|\psi_t\rangle = 1/\sqrt{2A} (1 - s_t i e^{i\theta_t})^T e^{i\mathbf{k}_t \cdot \mathbf{r}}$ where wavevector $k_t = \frac{|E+qV_p|}{\hbar v_F}$, θ_t is the transmission angle, t is the transmission coefficient and $s_t = \text{sgn}(E + qV_p)$. Since the potential along \hat{y} is uniform, the \hat{y} component of wavevector must be conserved throughout the device. Thus, we recover Snell's law for TI surface state: $k_i \sin \theta_i = k_t \sin \theta_t$. It follows from Snell's law and the opposite helicity of conduction and valence bands of TI surface states that the transmission angle $\theta_t = \pi - \theta'_t$ for $E < -qV_p$ and $\theta_t = \theta'_t$ for $E > -qV_p$ where $\theta'_t = \sin^{-1} \left[\frac{E+qV_p}{E+qV_p} \sin \theta_i \right]$. For electrons with $\theta_i > \theta_c \equiv \sin^{-1} \left[\frac{E+qV_p}{E+qV_n} \right]$, θ_t becomes complex and the electrons are reflected back to the source.

Inside the junction interface ($-d/2 < x < d/2$), the wavevector varies in accordance with $k(x) = \frac{|E-V(x)|}{\hbar v_F}$. For electrons with $k(x) < k_i \sin \theta_i$, the \hat{x} component of $\mathbf{k}(x)$ becomes imaginary, the wavefunctions become evanescent and the electrons are reflected back. Considering the exponential decay inside the interface and matching the wavefunction across an abrupt pn junction, the transmission coefficient can be written as $t = \frac{s_i e^{i\theta_i} + s_t e^{-i\theta_i}}{s_i e^{-i\theta_i} + s_t e^{i\theta_t}} e^{-\phi}$ where $\phi = \int \kappa(x) dx$ and $\kappa(x) = \sqrt{k_i^2 \sin^2 \theta_i - k^2(x)}$ is the imaginary part of $\mathbf{k}(x)$.

Now, let us consider an electron injected from the source at angle θ_i and energy E is transmitted from n to p and collected at drain. The probability current density for the transmitted electron is given by $J_{qt}(E, \theta_i) = |t|^2 \langle \psi_t | \hat{J}^x | \psi_t \rangle$ which leads to the general expression for the charge current density

$$J_q(E, \theta_i) \equiv J_{qt} = \frac{stqv_F}{A} |t|^2 \cos \theta_{tr} e^{-\theta_{ti}} e^{-\kappa_t L}, \quad (2)$$

where $\theta_{tr} = \text{Re}\{\theta_t\}$, $\theta_{ti} = \text{Im}\{\theta_t\}$ and $\kappa_t = \text{Im}\{\hat{x} \cdot \mathbf{k}_t\}$. Similarly, the probability current density for the incident wave is $J_{qi}(E, \theta_i) = s_i qv_F \cos \theta_i / A$. Hence, the transmission probability is given by $T(E, \theta_i) \equiv J_{qt} / J_{qi} = \frac{\cos \theta_{tr}}{\cos \theta_i} |t|^2 e^{-\theta_{ti}} e^{-\kappa_t L}$, which is the general form of transmission probability in graphene pn junction as presented in Refs. [2, 4] and valid for all energies in nn , pn and pp regime. Similarly, the spin current density at drain is

$$J_{syD}(E, \theta_i) = -\frac{\hbar v_F}{2A} |t|^2 e^{-2\theta_{ti}} e^{-\kappa_t L}, \quad (3)$$

where the negative sign indicates that the spin current is carried by the down spin. The spin current at source has two components: (1) the incident current $J_{syi}(E, \theta_i) = -\frac{\hbar v_F}{2A}$ and the reflected current $J_{syr}(E, \theta_i) = -\frac{\hbar v_F}{2A} |r|^2$. Therefore, the total spin current density is,

$$J_{syS}(E, \theta_i) = -\frac{\hbar v_F}{2A} (1 + |r|^2) \quad (4)$$

where $|r|^2 = 1 - |t|^2$. Eqs. 2-4 are valid for all energies in nn , pn and pp regimes. The total current is the sum of contributions from all electrons with positive group velocity along \hat{x} , weighted by the Fermi functions and integrated over all energies as given by Eq. S3. Unlike the incident and reflected components of charge currents, J_{syi} and J_{syr} have the same sign. This is because when a spin-up electron is reflected from the pn junction interface, its spin is flipped due to the spin-momentum locking. Now, a spin-down electron going to the left has the same spin current as a spin-up electron going to the right. Hence, the spin currents due to the injected and the reflected electron add up enhancing the source spin current.

For symmetric pn junction, within the barrier ($-qV_n < E < -qV_p$), the transmission coefficient is dominated by the exponential term and becomes $t \approx e^{-\pi\hbar v_F k_i^2 d \sin^2 \theta_i / 2V_o}$. Hence, t is nonzero for electrons with very small incident angle ($\theta_i \ll \theta_c$). For these electrons, $e^{-\theta_i} \approx 1$, $e^{-\kappa_i L} \approx 1$ and $\cos \theta_i \approx \cos \theta_{tr}$. Therefore, the transmission probability becomes,

$$T(E, \theta_i) \approx e^{-\pi\hbar v_F k_i^2 d \sin^2 \theta_i / V_o} \quad (5)$$

which has the same form as the transmission probability in graphene pn junction[2, 4]. The charge current density in symmetric pn junction is then,

$$J_q(E, \theta_i) \approx q \frac{v_F}{A} [1 - R(E, \theta_i)] \quad (6)$$

and spin current densities at drain and source are

$$J_{syD,S}(E, \theta_i) \approx -\frac{\hbar v_F}{2A} [1 \mp R(E, \theta_i)] \quad (7)$$

where $-$ and $+$ signs are for D and S respectively, and $R(E, \theta_i) = 1 - T(E, \theta_i)$ is the reflection probability. Now, the spin-charge current gain can be expressed as $\beta(E_F) = \int d\theta 2q J_{syS}(E_F, \theta) / \int d\theta \hbar J_q(E_F, \theta)$ in the low bias limit. For symmetric pn junction, β at the source contact reduces to the first expression in Eq. 1 where $R_{av} = \frac{1}{\pi} \int d\theta [1 - e^{-\pi\hbar v_F k_i^2 d \sin^2 \theta_i / V_o}]$ is the average reflection probability. When the Fermi energy is at the middle of the barrier, $\hbar v_F k_F = V_o/2$ and β is given by the second term of Eq. 1.

Eq. 5 clearly shows that $T(E, \theta_i)$ is nonzero only for electrons with very small θ_i . Hence, only these electrons are allowed to transmit. For all other modes, the reflection probability $R(E, \theta_i) \approx 1$ and those electrons are reflected back from the pn junction interface to the source. Thus, only few modes with small θ_i contribute to J_{syD} and J_q , whereas all other modes contribute to J_{syS} as shown in the inset of Fig. 3. This is also consistent with the spin polarization of TIPNJ shown in the inset of Fig. 2 calculated using NEGF with negligible injection from the drain. In the p side, only the transmitted waves exist and the spins of these electrons are aligned to $-\hat{y}$ due to the spin-momentum locking. Therefore,

the p side is highly spin polarized as illustrated by blue. On the other hand, in the n side, both the incident and the reflected waves exist with spins aligned to all the directions in $x - y$ plane leading to the unpolarized n region indicated by green. This is completely different from the uniform nn or pp device where the spin polarization is $2/\pi$ throughout the channel[27, 28]. Thus, the spin polarization shown in Fig. 2 is a key signature of spin filtering and amplification effect in TIPNJ, which can be measured by spin resolved scanning tunneling microscopy.

One way to measure β is to pass the spin current through a ferromagnetic metal (FM) by using the FM as the source contact of TIPNJ. The magnetization of the FM needs to be in-plane so that it does not change the TI bandstructure. The spin current going through the FM will exert torque on the FM which can be measured indirectly using spin torque ferromagnetic resonance technique[14] or directly by switching the magnetization (along $-\hat{y}$) of soft ferromagnets such as $(\text{Cr}_x\text{Bi}_y\text{Sb}_{1-x-y})_2\text{Te}_3$ at low temperature[15]. Once the magnetization of the FM is switched from $-\hat{y}$ to $+\hat{y}$, the current injection will stop (since spin up states cannot move towards right) and the system will reach the stable state.

In summary, we have shown that the chiral tunneling of helical states leads to an large spin-charge current gain due to the simultaneous amplification of spin current and suppression of charge current in a 3D TIPNJ. The chiral tunneling allows only the near normal incident electrons to transmit, suppressing the charge current significantly. The rest of the electrons are reflected and their spins are flipped due to the spin-momentum locking, enhancing the spin current at the source end. The gain at drain, however, remains close to one and the spin polarization becomes $\sim 100\%$. Any gate controllable, helical Dirac-Fermionic pn junction should exhibit a giant spin-charge current gain which may open a new way to design spin-tronic devices.

This work is supported by the NRI INDEX. The authors acknowledge helpful discussions with Y Xie (UVa), A Naeemi (Georgia Tech) and JU Lee (SUNY, Albany).

SUPPLEMENTAL

NEGF AND K.P METHOD

The discrete points in Figs. 2-3 (of main text) were calculated using the non-equilibrium Green's function (NEGF) formalism and the discretized k.p Hamiltonian, which captures the effects of edge reflections. Here we describe the calculation method.

The low energy effective Hamiltonian to describe the

surface states of TI has been shown to be[29]

$$H = v_F \hat{z} \cdot (\boldsymbol{\sigma} \times \mathbf{p})$$

where \mathbf{p} is the momentum, $\boldsymbol{\sigma} = (\sigma^x, \sigma^y)$ are the Pauli matrices, and v_F is the Fermi velocity of electron on the TI surface state. To avoid the well known fermion doubling problem[30, 31] on discrete lattice, we added a σ^z term to this Hamiltonian,

$$H = v_F \hat{z} \cdot (\boldsymbol{\sigma} \times \mathbf{p}) + \gamma \sigma^z (k_x^2 + k_y^2)$$

as suggested in Refs. [28 and 31]. This k-space Hamiltonian is transformed to a real-space Hamiltonian by replacing k_x with differential operator $-i\frac{\partial}{\partial x}$, k_x^2 with $-\frac{\partial^2}{\partial x^2}$ and so on. The differential operators are then discretized in a square lattice using finite difference method to obtain the translational invariant, real-space Hamiltonian,

$$H = \sum_i c_i^\dagger \epsilon c_i + \sum_i \left(c_{i,i}^\dagger t_x c_{i,i+1} + \text{H.C.} \right) + \sum_j \left(c_{j,j}^\dagger t_y c_{j,j+1} + \text{H.C.} \right) \quad (\text{S1})$$

where $\epsilon = -4\hbar v_F \frac{\alpha}{a} \sigma^z$, $t_x = \hbar v_F \left[\frac{i}{2a} \sigma^y + \frac{\alpha}{a} \sigma^z \right]$, $t_y = \hbar v_F \left[-\frac{i}{2a} \sigma^x + \frac{\alpha}{a} \sigma^z \right]$, a is the grid spacing and $\alpha \equiv \gamma a$ is a fitting parameter. For a grid spacing of $a = 5 \text{ \AA}$, the fitting parameter $\alpha = 1$ generates a bandstructure that reproduces the ideal linear bandstructure within a large energy window ($\sim \pm 0.5 \text{ eV}$) and gets rid of the Fermion doubling problem. The discretized, real-space Hamiltonian given by Eq. S1 with parameters $\alpha = 1$ and $a = 5 \text{ \AA}$ is used for all of our NEGF calculations.

In order to calculate the charge and spin currents, we adopted the current density operator[32, 33],

$$I_{op} = \frac{1}{\hbar} \left\{ G^n \Sigma_m^\dagger - \Sigma_m G^n + G \Sigma_m^{in} - \Sigma_m^{in} G^\dagger \right\} \quad (\text{S2})$$

where G^n is the electron correlation function, Σ_m is the self-energy of contact $m \in \{S, D\}$ and Σ_m^{in} is the in scattering matrix. The charge and spin currents are then given by, $I_q(E) = q \text{Tr} \{ I_{op} \}$ and $I_s(E) = \frac{\hbar}{2} \text{Tr} \{ \boldsymbol{\sigma} I_{op} \}$ respectively. Since equilibrium spin current exists on the TI surface[20, 21], this spin current includes both equilibrium and non-equilibrium components. In order to obtain the non-equilibrium spin current, first we calculate equilibrium spin current, I_{s_0} by setting $\mu_S = \mu_D = 0$ where, μ_S and μ_D are chemical potentials of the source and the drain contacts respectively. Then we calculate total (equilibrium + non-equilibrium) spin current I_s by setting $\mu_D = 0$ and $\mu_S = qV_{DS}$. Finally, the total non-equilibrium spin current is obtained using $I_{s_{neq}}(E) = I_s(E) - I_{s_0}(E)$ and integrating over all energies.

We found that the additional σ^z term in Eq. S1 has an artifact. It gives a small non-zero I_{sx} and I_{sz} compared to zero values predicted by our analytical model using the exact Hamiltonian. However, this does not affect

our conclusions since the focus is on I_{sy} . Also, using the full 3D TI k.p Hamiltonian (described on the cubic lattice of a 3D TIPNJ slab) and the NEGF formalism, we verified that $I_{sx} = 0$ and $I_{sz} = 0$. Although the full k.p Hamiltonian gives more accurate results for I_{sx} and I_{sz} , it is computationally inefficient.

ANALYTICAL EXPRESSION FOR TOTAL CURRENT

The total current at energy E is the sum of contribution from all electrons with positive group velocity along \hat{x} , $I(E) = W \sum_{v_x(\mathbf{k}) > 0} J(E, \theta) \delta(E - E_{\mathbf{k}})$ where δ is the Dirac delta function and W is the width of the device. Replacing $\sum_{v_x(\mathbf{k}) > 0}$ with $\frac{A}{4\pi^2} \int_{v_x(\mathbf{k}) > 0} d^2k$ in this expression, using the delta function property $\delta(f(x)) = \frac{\delta(x-x_0)}{|f'(x_0)|}$ and integrating over all energy yield the general expression for total current,

$$I = \frac{W}{2\pi} \int dE D(E) [f_S(E) - f_D(E)] \int d\theta A J(E, \theta) \quad (\text{S3})$$

where, $D(E) = \frac{1}{2\pi} \frac{|E+qV_n|}{\hbar^2 v_F^2}$ is the density of states which has the units of $\text{eV}^{-1} \text{m}^{-2}$, and $f_S(E)$ and $f_D(E)$ are the Fermi-Dirac distributions of source and drain, respectively. Eqs. 2-4 (of main text) and Eq. S3 are valid for both symmetric and asymmetric built in potentials in nn , pn and pp regimes for all energies and hence can be used to calculate spin and charge current for large drain bias at room temperature. The solid lines of Figs. 2-3 were calculated using Eqs. 2-4 and Eq. S3.

THE ANGULAR SPIN CURRENT \mathbf{J}_ω

It can be shown that the spin current operator that describes the angular motion/precession of spin in a 3D TI surface is given by

$$\hat{\mathbf{J}}_\omega = \hbar v_F [-k_x \sigma^z \hat{x} - k_y \sigma^z \hat{y} + (k_x \sigma^x + k_y \sigma^y) \hat{z}]. \quad (\text{S4})$$

The expectation value of $\hat{\mathbf{J}}_\omega$ for the TI surface eigenstate $|\psi\rangle = 1/\sqrt{2A} (1 - \text{sie}^{i\theta})^T e^{i\mathbf{k}\cdot\mathbf{r}}$ is $\mathbf{J}_\omega = \mathbf{0}$. Therefore, for a uniform TI channel where there is no scattering, the spin continuity equation becomes $\nabla \cdot \mathbf{J}_s = \mathbf{0}$ in the steady state and the spin current is conserved. More intuitively, in a uniform TI channel, the momentum of an electron does not change with time. Since the spin and momentum are locked, the spin angular momentum also remains constant. Thus, there is no rotation/precession in spin and therefore, $\mathbf{J}_\omega = \mathbf{0}$ and the spin current is conserved.

Similarly, in the TIPNJ, the spin current is conserved inside the channel under the gates G1 and G2 where the potential profile is uniform. When an electron is reflected

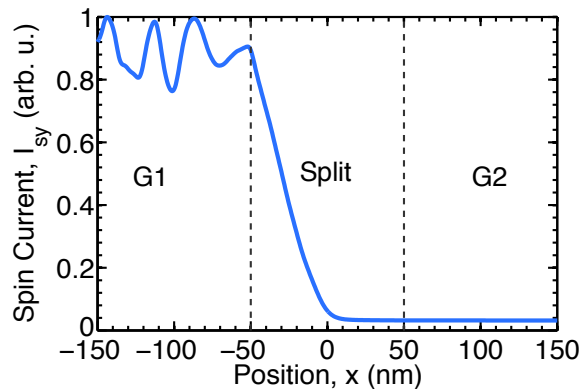


FIG. S1. Spin current density as a function of position calculated using NEGF. Spin current is constant in the G2 (p) region. The small oscillation in G1 (n) region is due to interference created by reflected waves from the edges. The large change in the Split region is due to rotation/precession of spin when electrons are reflected. In this simulation, we have used larger gates (100nm compared to 10nm in the original calculations) to illustrate the conservation of spin current in the uniform gate regions.

at the pn junction interface, the direction of momentum changes by $\pi - 2\theta_i$ accompanied by the same amount of change in the direction of spin angular momentum. In this case $\mathbf{J}_\omega \neq \mathbf{0}$ and the spin current is no longer conserved. The change in the spin angular momentum created by the reflection generates the spin torque.

This is also consistent with the spatial variation of spin current along the device calculated using NEGF as shown in Fig. S1. Since there is no potential variation under the gates G1 and G2, there is no scattering and the spin current remains mostly conserved in these regions. The small oscillatory change in the G1 region is due to the interference created by the edge reflection in a finite-width device which is not included in the analytical model. The interference pattern can also be seen in the spin polarization plot in Fig. 2. On the other hand, inside the linear region, the electrons change direction which, in turn, results in a change in spin angular momentum. Therefore, spin current is not conserved. We also verified using NEGF that $I_{syS} - I_{syD} = I_{sy\omega}$ where, $I_{sy\omega} = \int J_{sy\omega} dS$, and I_{syS} and I_{syD} are the total spin currents at source and drain, respectively. Therefore, the difference between the spin currents at the source and the drain terminal is the spin torque generated by the TIPNJ.

In our analytical model, the effects of non-zero \mathbf{J}_ω inside the linear region are taken into account by constructing correct wave functions for the reflected and the transmitted waves. Given the correct wavefunctions, Eqs. (3) and (4) give correct spin currents everywhere for $x < -d/2$ and $x > d/2$ (neglecting the small oscillation due to edge reflections) since the spin current is conserved in these regions. In NEGF, the effects of \mathbf{J}_ω are taken

into account automatically by the device Hamiltonian.

* masum.habib@virginia.edu

- [1] X.-L. Qi and S.-C. Zhang, *Reviews of Modern Physics* **83**, 1057 (2011).
- [2] V. V. Cheianov and V. I. Fal'ko, *Phys. Rev. B* **74**, 041403 (2006).
- [3] A. F. Young and P. Kim, *Nat Phys* **5**, 222 (2009).
- [4] R. N. Sajjad, S. Sutar, J. Lee, and A. W. Ghosh, *Physical Review B* **86**, 155412 (2012).
- [5] R. N. Sajjad and A. W. Ghosh, *ACS nano* **7**, 9808 (2013).
- [6] Z. Wu, F. Peeters, and K. Chang, *Appl. Phys. Lett.* **98**, 162101 (2011).
- [7] R. Takahashi and S. Murakami, *Phys. Rev. Lett.* **107**, 166805 (2011).
- [8] J. Wang, X. Chen, B.-F. Zhu, and S.-C. Zhang, *Physical Review B* **85**, 235131 (2012).
- [9] S. Datta, V. Q. Diep, and B. Behin-Aein, "What Constitutes a Nanoswitch? A Perspective," in *Emerging Nanoelectronic Devices*, edited by A. Chen, J. Hutchby, V. Zhirnov, and G. Bourianoff (John Wiley and Sons, 2015) Chap. 2, p. 22.
- [10] L. Liu, C.-F. Pai, Y. Li, H. W. Tseng, D. C. Ralph, and R. A. Buhrman, *Science* **336**, 555 (2012).
- [11] S. Datta, S. Salahuddin, and B. Behin-Aein, *Applied Physics Letters* **101**, 252411 (2012).
- [12] O. Mosendz *et al.*, *Phys. Rev. Lett.* **104**, 046601 (2010).
- [13] L. Liu, T. Moriyama, D. C. Ralph, and R. A. Buhrman, *Phys. Rev. Lett.* **106**, 036601 (2011).
- [14] A. Mellnik *et al.*, *Nature* **511**, 449 (2014).
- [15] Y. Fan *et al.*, *Nature Materials* **13**, 699 (2014).
- [16] J.-H. Gao, J. Yuan, W.-Q. Chen, Y. Zhou, and F.-C. Zhang, *Phys. Rev. Lett.* **106**, 057205 (2011).
- [17] S. Manipatruni, D. E. Nikonov, and I. A. Young, *Applied Physics Express* **7**, 103001 (2014).
- [18] J. Lee, J.-H. Lee, J. Park, J. S. Kim, and H.-J. Lee, *Phys. Rev. X* **4**, 011039 (2014).
- [19] J. Chen *et al.*, *Phys. Rev. Lett.* **105**, 176602 (2010).
- [20] A. A. Burkov and D. G. Hawthorn, *Phys. Rev. Lett.* **105**, 066802 (2010).
- [21] Y. Tserkovnyak and D. Loss, *Phys. Rev. Lett.* **108**, 187201 (2012).
- [22] E. I. Rashba, *Phys. Rev. B* **68**, 241315 (2003).
- [23] I. V. Tokatly, *Phys. Rev. Lett.* **101**, 106601 (2008).
- [24] E. B. Sonin, *Phys. Rev. Lett.* **99**, 266602 (2007).
- [25] F. MAHFOUZI and B. K. NIKOLI, *SPIN* **03**, 1330002 (2013).
- [26] Q.-f. Sun and X. C. Xie, *Phys. Rev. B* **72**, 245305 (2005).
- [27] O. V. Yazyev, J. E. Moore, and S. G. Louie, *Phys. Rev. Lett.* **105**, 266806 (2010).
- [28] S. Hong, V. Diep, S. Datta, and Y. P. Chen, *Phys. Rev. B* **86**, 085131 (2012).
- [29] Y. Zhang, T.-T. Tang, C. Girit, Z. Hao, M. C. Martin, A. Zettl, M. F. Crommie, Y. R. Shen, and F. Wang, *Nature* **459**, 820 (2009).
- [30] R. Stacey, *Phys. Rev. D* **26**, 468 (1982).
- [31] L. Susskind, *Phys. Rev. D* **16**, 3031 (1977).
- [32] A. N. M. Zainuddin, S. Hong, L. Siddiqui, S. Srinivasan, and S. Datta, *Phys. Rev. B* **84**, 165306 (2011).
- [33] See Eq. 8.6.5, p. 317 in S. Datta, *Electronic Transport in Mesoscopic Systems*, Cambridge University Press, Cambridge, England (1997).